The Laryngoscope

Second Harmonic Imaging of Nasal, Auricular, and Costal Cartilage

Katelyn K. Dilley, BS; Akarsh Lal, BS; Theodore V. Nguyen, BS; Brian J. F. Wong, MD, PhD

Objective: There is little knowledge about the histological organization of facial and costal cartilages in terms of matrix structure and cell morphology. Second harmonic generation (SHG) imaging is a nonlinear imaging technique that capitalizes on signal generation from highly ordered macromolecules such as collagen fibers. The purpose of this study was to use SHG microscopy to image collagen extracellular matrix (ECM) structure, chondrocyte size, and density of these cartilages.

Study Design: Experimental.

Methods: Surgical remnants of septal, lower lateral, rib, and auricular cartilages were collected following surgery, sectioned into 0.5–1 mm thick samples and fixed to facilitate batch process imaging. A Leica TCS SP8 MP Microscope and multiphoton laser were used to image the specimens. Images were analyzed for cell size, cell density, and collagen fiber directionality patterns using ImageJ.

Results: SHG images of septal specimens show mesh-like structure of the ECM. There appears to be a superficial layer, characterized by flattened lacunae and middle zone, marked by circular lacunae clusters, similar to what is observed in articular cartilage. The structure of the ECM depicts a visible orientation perpendicular to the surface of the perichondrium. Cell size and density analysis through ImageJ suggests variety across cartilage types. Directionality analysis indicates that the collagen in the ECM displays preferred direction.

Conclusion: This study establishes clear extracellular models of facial and costal cartilages. Limitations include heterogeneous cartilage thickness due to processing difficulties. Further studies include automating the cutting process to increase uniformity of tissue thickness and increasing sample size to further validate results.

Key Words: facial plastics/reconstructive surgery, basic research, basic science research.

Level of Evidence: 2

***Laryngoscope*, 133:3370–3377, 2023**

INTRODUCTION

Cartilage lines articular surfaces, provides flexure and shock absorbance for the joints and vertebrae, supports the airway, and provides shape to the structures of the face.[1] Classically, cartilage is divided into three categories: elastic cartilage, fibrocartilage, and hyaline cartilage. Hyaline cartilage has a white, glass-like appearance and is located between the ends of bones in joints, at the ends of the ribs, and in the nose.[2]

Of these three types of cartilages, hyaline cartilage in the joints (articular cartilage) has been the focus of research aimed at understanding the microscopic structure and physiology of this tissue, whereas much less is known about other cartilage tissues, and even less is known about the native structure of the collagens in cartilage. Historically, collagen matrix structure has been examined using electron microscopy, but these methods are complex and require ultrathin tissue sectioning or dehydration and gold coating. One emerging microscopy technique used to study native collagen structure is second harmonic generation (SHG) imaging. SHG microscopy provides high-resolution (~350–400 nm), depth-resolved imaging of living tissue without the need for thin sectioning in a microtome, fixation, and staining such as that needed in classic light microscopy. A small number of studies have used SHG microscopy to image articular cartilage and shown the hierarchical structure of this tissue without any fixation artifact.[3]

Although there are extensive studies on the structure of cartilage in the joints, little is known about the structure of collagen and the extracellular matrix (ECM) of facial and costal cartilages; our current understanding of morphologic cartilages, such as septal cartilage, predicates on inferences through other studies.[4]

In this study, we examined septal, auricular, costal, and lower lateral (alar) cartilage specimens, the principal cartilages used in rhinoplasty and nasal reconstruction operations, using second harmonic generation microscopy to image type II collagen in the ECM. Additionally, the size and density of chondrocytes was measured, and collagen directionality was calculated.

From the Beckman Laser Institute and Medical Clinic (K.K.D., A.L., T.V.N., B.J.F.W.), Irvine, California, U.S.A.; Department of Otolaryngology—Head and Neck Surgery (B.J.F.W.), University of California—Irvine Medical Center, Orange, California, U.S.A.; and the Department of Biomedical Engineering (B.J.F.W.), Henry Samueli School of Engineering, Irvine, California, U.S.A.

Editor's Note: This Manuscript was accepted for publication on May 22, 2023.

Katelyn K. Dilley and Akarsh Lal contributed equally to this project.

The authors have no funding, financial relationships, or conflicts of interest to disclose.

Triological Society Combined Sections Meeting 2023. January 26–28, 2023.

Send correspondence to Brian J. F. Wong, MD, PhD, Department of Otolaryngology–Head and Neck Surgery, University of California, Irvine Medical Center, 101 The City Dr South, Orange, CA 92868.

Email: bjwong@uci.edu

DOI: 10.1002/lary.30803

MATERIALS AND METHODS

Tissue Collection, Fixation, and Preparation

Remnant surgical specimens (septal, auricular, costal, and lower lateral (alar) cartilages), approved by the University of California, Irvine institutional review board (IRB no. 20173708), acquired from rhinoplasty operations, were fixed in 10% buffered formalin. The samples were then transferred to 95% dehydrant. The fixed tissue was cut with a razor blade to create 0.5–1 mm-thick cross-sectional slices for SHG imaging. The cross-sectional slices were kept moist in PBS on a glass slide and then placed onto the microscope stage to be imaged.

Second Harmonic Generation Imaging

The tissue was imaged using a Spectra-Physics Insight Tunable Ultrafast laser (MKS Instruments, Milpitas, CA), with an excitation wavelength of 810 nm and an emission wavelength of 405 nm, in tandem with a custom built Leica TCS SP8 MP microscope (Leica Microsystems, Wetzlar, Germany) set to a detection range of 395–415 nm. The excitation wavelength was 810 nm because collagen is the contrast agent.[5] The surface of each cross-sectional slice was placed flush onto a glass slide. Images were captured using a 10× and 20× objective at 2048 × 2048 resolution.

Directionality, Cell Size, and Cell Density Analysis

The SHG images were first converted to 8-bit grayscale images in FIJI, an open source software for image processing.[6] Regions of interest (ROIs) for image acquisition were manually selected where SHG signal and details of the ECM were evenly distributed. The collected SHG images were analyzed for directionality patterns using the Directionality tool in FIJI, which detects the presence of preferred orientation of organized structures such as collagen fibrils present in an image.[7]

The method used for directionality analysis was "Fourier components" in FIJI, which divides an image into square sections and determines their Fourier power spectra. The output of the analysis provides a "Directionality" histogram. If a preferred orientation of structures is detected by the software, it is indicated with a peak in the histogram. The peak of the histogram is fitted by a Gaussian curve and indicates the angle at which the structures are oriented. The analysis also provides the Direction (°) (the center of the Gaussian) and the Dispersion (°) (the standard deviation of the Gaussian). This orientation angle is arbitrary, as none of the specimens are traced back to their anatomic orientation, and no attempt at registry was made with the surgical specimens.

Cell count in high-power images were performed manually by using the "Cell Counter" function in ImageJ, and density was calculated as cells per unit area squared. Images were vertically bisected, and the left half of each SHG image was analyzed for finding cell size. In each image, cells were manually outlined,

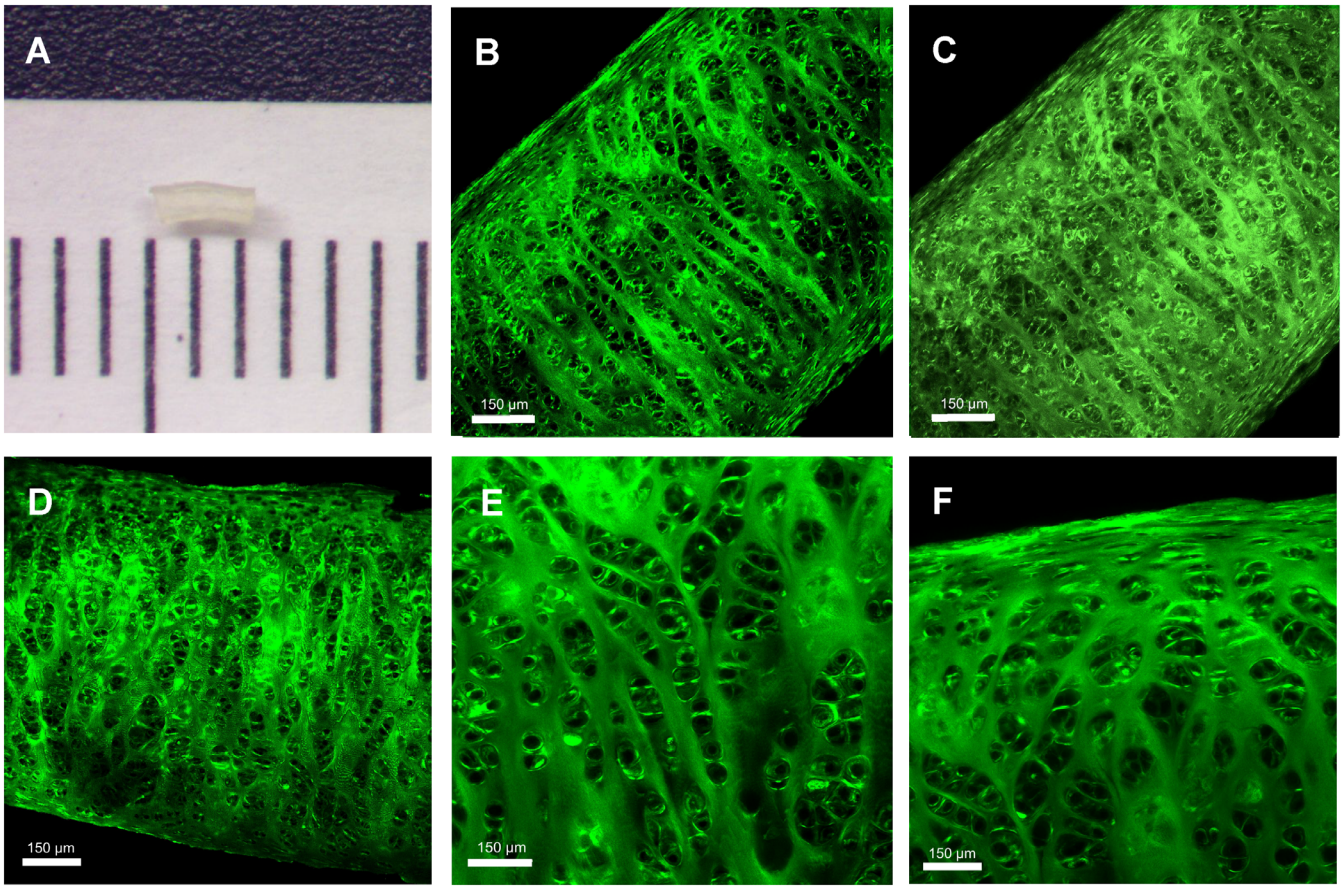

Fig. 1. (A) Digital image of the ~2 mm long septum specimen and (B, C, and D) SHG images at 10× magnification of the specimen. (E and F) SHG snapshots at 20× magnification of a subsection of the region imaged in (B).

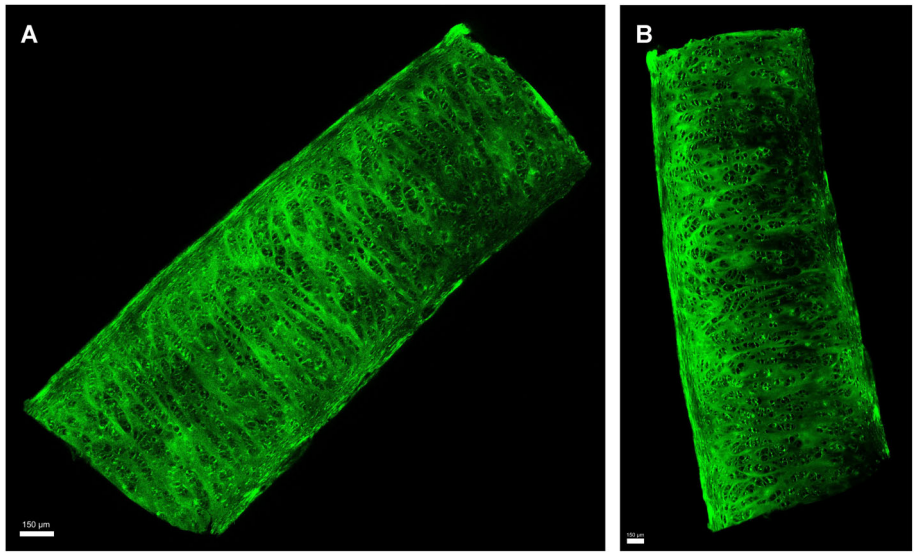

Fig. 2. SHG tilescans at 10× magnification of cut cross sections of septal cartilage specimen.

and the "Analyze Particles" tool in ImageJ calculated the area of each cell. Statistical analysis was performed on IBM SPSS statistics (Version 28, IBM Corp., Armonk, NY).

RESULTS

High-resolution photographs of the septal specimen show the characteristic white, glass-like appearance

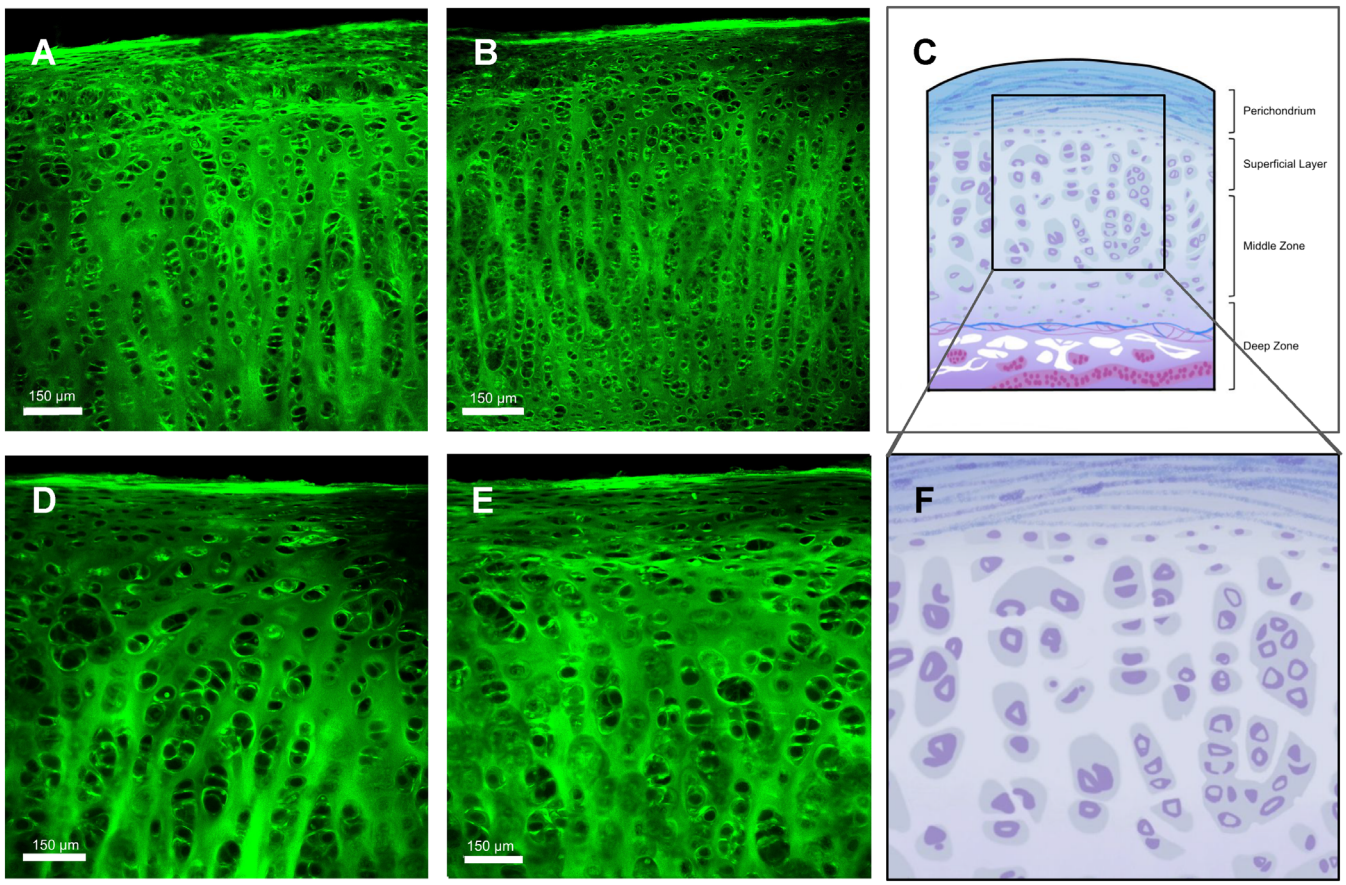

Fig. 3. Cross-sectional SHG images of septal cartilage at 10× magnification (A, B) and 20× magnification (D, E). A schematic illustration exhibiting the superficial layer, middle zone, and deep zone of articular cartilage is shown in C and F.

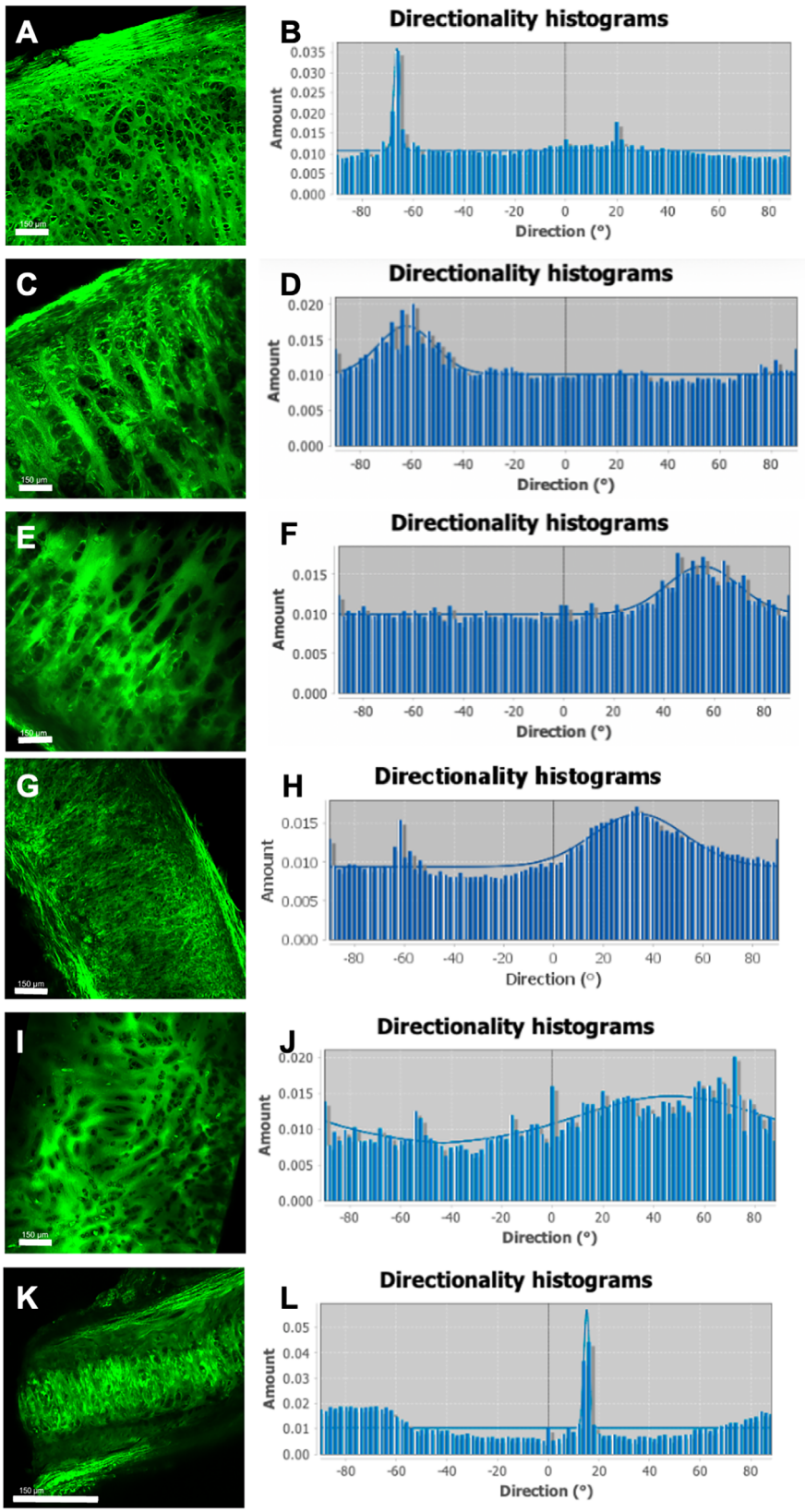

Fig. 4. SHG snapshots at 10× magnifications of three different (A, C, and E) septum specimens, (G) auricular cartilage, (I) costal cartilage, and (K) lower lateral cartilage adjacent to their corresponding directionality histograms (B, D, F, H, J, and L), respectively. The direction of the structures in the images is measured in degrees (°) on the *x*-axis and the amount is a unitless measurement on the *y*-axis.

TABLE I.
Quantitative Values for Direction (°) and Dispersion (°) for the Six Directionality Histograms.

Image	Cartilage	Direction (°)	Dispersion (°)
Figure 4B	Septal	−66.25	1.27
Figure 4D	Septal	−62.18	10.97
Figure 4F	Septal	55.83	14.37
Figure 5B	Auricular	34.19	18.57
Figure 5D	Costal	46.98	36.09
Figure 5F	Lower lateral	15.15	1.07

characteristic of hyaline cartilage (Fig. 1A). Composite SHG tilescans of these specimens show the mesh-like structure of the ECM (Fig. 2). In general, septal cartilage is relatively flat over small spatial scales, though macroscopically it may be deformed from trauma, surgery, or infection. Curvature of a specimen may result in the shifts in the image plane and loss of signal. This can be compensated for by imaging across smaller ROIs. Although the majority of the image planes selected were in regions where the specimen was flat, there are still some areas of signal loss which may be a consequence of imprecision in sectioning or warping during the section process. Septal cartilage images include remnants of perichondrium, which may have been incompletely removed by clinicians, as indicated by the band-like orientation of stacked cells at the periphery (Fig. 1B, C). Macroscopically, a specimen may be clinically free of perichondrium, though microscopically a small layer may persist. Notably at higher magnification (20×), collagen signal is identified between lacunae (Fig. 1E, F). The homogeneous appearance of the ECM and the absence of noticeable collagen fibers in the SHG images distinguishes the septal cartilage as hyaline cartilage, rather than fibrocartilage or elastic cartilage, in which the SHG signal is evident with fibrillar structures (Fig. 1).

Figure 3 compares the SHG images of septum with the known structure of articular cartilage. Although the structure and biology of articular cartilage is profoundly different, descriptive terminology may have some value with regard to the images we observe in septal cartilage. The superficial layer and middle zone are apparent in the SHG images and similar in structure to previous histology of articular cartilage. The superficial layer is characterized by flattened lacunae (black "holes" in the SHG images) and transitions into the middle zone, which is marked by circular lacunae appearing in clusters.[8,9] The territorial matrix, marked by the increased intensity of bright signals surrounding the lacunae, is also seen in Figure 3. The lacunae are present as both clusters and as singular lacunae. The perichondrium is marked by the bright linear signal at the edge of the SHG images in Figure 3.

The SHG images at the periphery of the septal cartilage specimen demonstrate that there are structural changes both to the density and morphology of the chondrocytes, as well as the surrounding ECM. There is a change in cell size from being compressed, flattened, and dense to being more circular; this occurs as one goes deeper axially into the specimen. The classic appearance associated with septal cartilage is seen in the central parts of the specimen, and one can see an almost band-like distribution of cells with the vertical stacking of chondrocytes separated from other populations by homogeneous regions of matrix.

Clusters of cells and the ECM are both stacked and segregated into these linear structures that run perpendicular to the perichondrial surface. Directionality analysis through ImageJ further indicates that the collagen in the ECM also displays a preferred direction. The directionality histograms for three different septal specimens show the measured direction angle and relative magnitude (Fig. 4B, D, F). There is a preferred orientation of the ECM, marked by the distinct peak in each histogram. The direction (°) at which the peaks are present is arbitrary because each image would produce a different peak if it were to be rotated.

Figure 4G–L provide a side-by-side comparison of auricular, costal, and lower lateral cartilages. The lacunae in auricular and lower lateral cartilages (Fig. 4G, K) are grouped into clusters arranged in a stacked band-like pattern, whereas the costal cartilage lacunae (Fig. 4I) are more arbitrary in distribution and less tightly packed, with no distinct orientation. Perichondrium is visible and marked by a bright linear signal surrounding the outer edge of the septal, auricular, and lower lateral cartilages. Remnants of perichondrium can be observed in all three types of cartilages, but are more prominent in lower lateral and auricular cartilages.The ECM and chondrocytes of both lower lateral and auricular cartilages are also linearly aligned and stacked and have a visible orientation that is perpendicular to the surface of the perichondrium. These features are similar to that of the septal SHG images. However, septal cartilage demonstrates greater banded organization of the ECM and larger, distinct lacunae in comparison with those of lower lateral cartilage.[10] In contrast, costal cartilage lacunae are less regularly shaped, and the ECM has an irregular mesh which does not demonstrate visible orientation. There is no enhanced signal intensity surrounding the lacunae to suggest the potential presence of the territorial matrix.

Figure 4H, L shows that the ECM of auricular cartilage and lower lateral cartilage are clearly oriented because their directionality histograms show distinct peaks at 34.19° and 15.15°, respectively (Table I). In contrast, the costal cartilage directionality histogram does not have a distinct peak (Fig. 4J). Table I shows that Figure 4J has the largest dispersion of the three images, whereas all three septal cartilage SHG images (Fig. 4B, D, F) have dispersions less than 15°, indicating a greater variation in the directionality of costal cartilage ECM than that of septal cartilage ECM.

In addition to comparing the SHG images and directionality of the different types of cartilages, cell density was determined to be significant on one-way ANOVA [F (3, 16) = 6.244; $p = 0.005$; Fig. 5A]. On post hoc analysis, septal cartilage (390.76 ± 38.30 cells/mm^2; $n = 8$) was

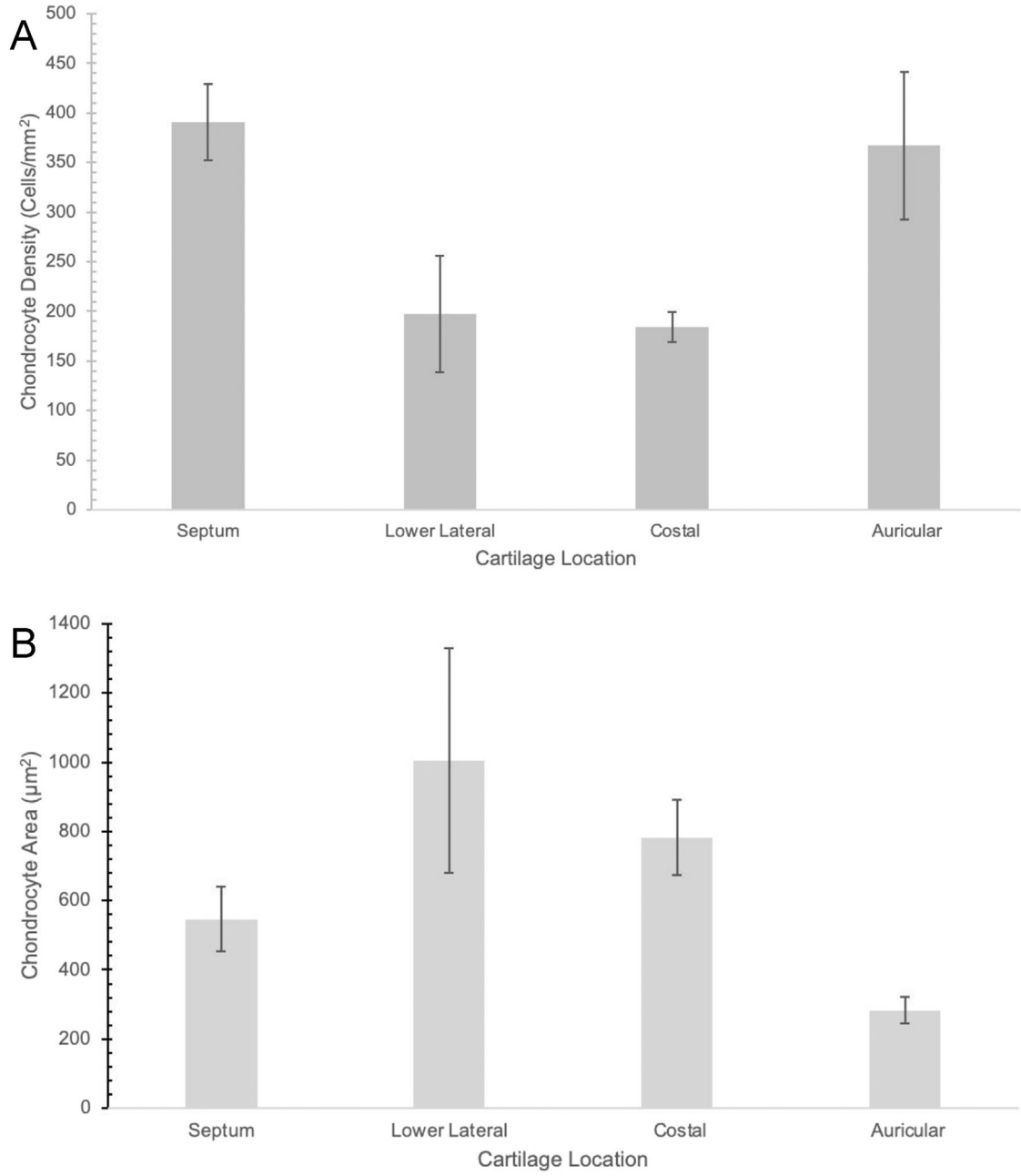

Fig. 5. (A) Chondrocyte density (cells/mm^2) of septal, lower lateral, costal, and auricular cartilages. Values are expressed as mean ± SEM. There were no significant differences between the four groups on one-way ANOVA [F (3, 16) = 6.244; p = 0.005]. (B) Chondrocyte area of septal, lower lateral, costal, and auricular cartilages. Chondrocyte area (µm^2) was measured on ImageJ. Values are expressed as mean ± SEM. There were no significant differences between the four groups on one-way ANOVA [F (3, 16) = 2.872; p = 0.069].

TABLE II.
Descriptive Statistics of Septal, Lower Lateral, Costal, and Auricular Cartilage for Density (cells/mm^2).

Cartilage Type	Mean Density (cells/mm^2) ± SEM
Septal (n = 8)	390.76 ± 38.30
Lower lateral (n = 4)	197.18 ± 58.75
Costal (n = 5)	184.01 ± 15.15
Auricular (n = 3)	365.36 ± 74.36

found to be significantly denser than lower lateral (197.18 ± 58.75; n = 4; p = 0.037) and costal cartilages (184.01 ± 15.15; n = 5; p = 0.014) [Tables II and III]. There were no other significant differences between the cell density of our samples. In regards to cell size, there were no significant differences on one-way ANOVA between septal (544.18 ± 91.95 µm^2; n = 8), lower lateral (1005.52 ± 325.38 µm^2; n = 4), rib (782.58 ± 109.69 µm^2; n = 5), or auricular cartilage (282.97 ± 37.37 µm^2; n = 3) cell areas [F (3, 16) = 2.907; p = 0.067; Fig. 5B].

TABLE III.
Post Hoc Analysis of One-Way ANOVA of Septal, Lower Lateral, Costal, and Auricular Cartilages' Cell Density (cells/mm^2).

Cartilage Type	Mean Difference	95% CI	*p*-Value
Septal ($n = 8$)			
Lower Lateral ($n = 4$)	**193.58 ± 61.49**	**8.60, 378.57**	**0.037**
Costal ($n = 5$)	**206.75 ± 57.24**	**34.53, 378.96**	**0.014**
Auricular ($n = 3$)	23.39 ± 67.98	−181.11, 227.91	1.000
Lower Lateral ($n = 4$)			
Costal ($n = 5$)	13.16 ± 67.36	−189.48, 215.81	1.000
Auricular ($n = 3$)	−170.19 ± 73.33	−400.91, 60.53	0.248
Costal ($n = 5$)			
Auricular ($n = 3$)	183.35 ± 73.33	−37.26, 403.96	0.142

Note: One-way ANOVA [F (3, 16) = 6.244; $p = 0.005$] was performed with Bonferonni post hoc analysis. Bolded values indicate significance set at $p < 0.05$. All mean differences are expressed as mean difference ± SEM.

DISCUSSION

This study analyzed ECM organization, cellular size, and cellular density of facial and costal cartilages. Previous studies have indicated that facial and costal cartilages are different from each other through the use of light microscopy.[11] However, through the use of SHG microscopy, we are the first to specifically visualize signal intensity of type II collagen to discern ECM differences between surgical remnant human facial and costal cartilages. It is important to note that individual collagen fibrils were not resolved because the size of the fibrils is smaller than the diffraction limit of optical microscopy.[12]

First, on analysis of cell density, it was shown that septal cartilage had significantly higher chondrocyte densities when compared with lower lateral or costal cartilage. However, there were no significant differences between septal and auricular cartilages. Additionally, there were no significant differences between lower lateral, costal, and auricular cartilages. On analysis of cell size, there were no significant differences between the four cartilage types.

SHG microscopy has been previously used to study articular cartilage and its repair mechanisms. Even more importantly, some suggest that septal and costal cartilages could be used to repair articular cartilage defects but acknowledge that there is lack of meaningful information on the ECM arrangement of these cartilages.[13] Knowing the structure of these facial cartilage tissues and the arrangement of the ECM could have potential importance for the development of tissue replacements for cartilage, whether native or engineered tissue.

In the acquired SHG images, several features of the ECM are noteworthy. The shape of the lacunae in septal, auricular, and lower lateral cartilages are similar; they are round and organized in clusters of multiple cells (Fig. 4A, C, E). In contrast, the lacunae in the costal cartilage have elongated and irregular shapes (Fig. 4G, I, K). A band-like, stacked arrangement of lacunae is also evident in the ECM of septal, auricular, and lower lateral cartilages, whereas costal cartilage lacks this pattern and has an interlacing, meshed ECM. The band-like, columnar arrangement in the septal, auricular, and lower lateral cartilages is oriented orthogonally to the surface of the perichondrium, which is supported by the directionality histograms indicating a preferred orientation of the ECM in these cartilages. This may indicate that these cartilages resist compressive forces predominantly along this direction.[14] In contrast, the interlacing ECM in costal cartilage may result from this cartilage resisting complex multidirectional forces and macroscopic displacements as part of the thorax. It has been previously shown that axial compression on costal chondrocytes enhanced the synthesis of ECM cartilage during a one-time stimulation.[15] Hence, a lack of preferred ECM orientation, indicated by the directionality histogram for costal cartilage, could indicate that costal chondrocytes produce ECM in multiple directions in response to compression. Further research is required to investigate this possibility. The dispersion values also highlight the greater degree of variation in orientation of costal cartilage in comparison with that of septal, auricular, and lower lateral cartilages. This depicts the variable structure of costal cartilage and relatively less varied structure of the other cartilages. These features may reflect the nuanced roles of septal, auricular, and lower lateral cartilages compared with those of costal cartilage in resisting physical compression and displacement, a key function of cartilage.[16] Additionally, the study of articular cartilage has revealed that the meshwork of the ECM serves to entrap proteoglycans to serve its mechanical resistive function.[17] A similar functionality may be present within the facial and costal cartilages. However, information about the placement and orientation of the entire cartilages in their natural environments would be needed to investigate this further.

The flattened lacunae adjacent to the perichondrium in septal, auricular, and lower lateral cartilages are also noteworthy. These are at the junction of the inner chondrogenic layer of the perichondrium and are the location of chondroblasts.[18] The band-like arrangement in the three cartilages may result from appositional growth of the cartilage, presumably during which chondroblasts mature into chondrocytes and move into the ECM.

Although this is a novel use of SHG to explore the structural differences of human septal, lower lateral (alar), auricular, and costal cartilages, there are several limitations that must be addressed. First, our tissue was fixed prior to imaging, which causes some information to be lost (NADH/NADPH as a contrast agent), but collagen signal intensity can still be seen. Another limitation includes the limited sampling of cartilage as tissue specimens are surgical remnants, and thus, there may be structural differences between the regions of the septum, lower lateral, and auricular cartilages that were not sampled. Remnant tissue from rhinoplasty operations is scarce, often irregular in geometry, and small in size. Fewer remnants of lower lateral and auricular cartilages are generally available compared with costal or septal cartilage. Hence, our current sample size is small with auricular cartilage having a sample size of 3. In future studies, sample size of each cartilage type must be increased to discern cell size and count differences between each tissue type.

Future studies should include developing a customized micro-guillotine device and adjusting the microscope stage brackets. This is due to SHG imaging requiring thin and evenly processed tissue, which is limited by human dexterity, and minute variations in the topology of the cleaved surface will create issues with signal dropoff and intensity. Further studies must be performed with larger sample sizes and larger remnant tissue to better discern differences between the four types of cartilages.

CONCLUSION

Herein, we explored the directionality, cell count, and cell sizes of auricular, lower lateral, costal, and septal cartilages in humans. This is the first study to perform SHG imaging and analysis on *ex vivo* surgical remnant human facial and costal cartilages. Previous literature has studied these cartilages using SHG imaging within a cadaveric model.[19,20] This present study described the differences between auricular, lower lateral, costal, and septal cartilages in human remnant surgical tissue and explored the usage of SHG in facial and costal cartilages. The study of facial and costal cartilages is a largely unexplored yet intriguing area of research. Examining the microscopic structure of these cartilages may lead to new avenues in the research of cartilage repair as well as help develop new microscopic models of the cartilage present in the human body. We may also gain a new understanding of the implications of these cartilages' interchangeable uses in head and neck surgeries.

ACKNOWLEDGEMENTS

We thank Naya Sterritt and Clara Chao for their contributions in data collection. Research reported in this publication was supported by the Office Of The Director, National Institutes Of Health of the National Institutes of Health, under Award Number S10OD028698. The content is solely the responsibility of the authors and does not necessarily represent the official views of the National Institutes of Health.

BIBLIOGRAPHY

1. Lau A, Oyen ML, Kent RW, Murakami D, Torigaki T. Indentation stiffness of aging human costal cartilage. *Acta Biomater*. 2008;4(1):97-103. https://doi.org/10.1016/j.actbio.2007.06.008.
2. Kheir E, Shaw D. Hyaline articular cartilage. *Orthop Trauma*. 2009;23(6):450-455. https://doi.org/10.1016/j.mporth.2009.01.003.
3. Boyanich R, Becker T, Chen F, Kirk TB, Allison G, Wu J-P. Application of confocal, SHG and atomic force microscopy for characterizing the structure of the most superficial layer of articular cartilage. *J Microsc*. 2019;275(3):159-171. https://doi.org/10.1111/jmi.12824.
4. Baddam P, Bayona-Rodriguez F, Campbell SM, El-Hakim H, Graf D. Properties of the nasal cartilage, from development to adulthood: a scoping review. *Cartilage*. 2022;13(1) 194760352210876. https://doi.org/10.1177/19476035221087696.
5. Zoumi A, Yeh A, Tromberg BJ. Imaging cells and extracellular matrix *in vivo* by using second-harmonic generation and two-photon excited fluorescence. *Proc Natl Acad Sci*. 2002;99(17):11014-11019. https://doi.org/10.1073/pnas.172368799.
6. Schindelin J, Arganda-Carreras I, Frise E, et al. Fiji: an open-source platform for biological-image analysis. *Nat Methods*. 2012;9(7):676-682. https://doi.org/10.1038/nmeth.2019.
7. Reznikov N, Almany-Magal R, Shahar R, Weiner S. Three-dimensional imaging of collagen fibril organization in rat circumferential lamellar bone using a dual beam electron microscope reveals ordered and disordered sub-lamellar structures. *Bone*. 2013;52(2):676-683. https://doi.org/10.1016/j.bone.2012.10.034.
8. Sophia Fox AJ, Bedi A, Rodeo SA. The basic science of articular cartilage: structure, composition, and function. *Sports Health Multidiscip Approach*. 2009;1(6):461-468. https://doi.org/10.1177/1941738109350438.
9. Hunziker EB, Quinn TM, Häuselmann HJ. Quantitative structural organization of normal adult human articular cartilage. *Osteoarthr Cartil*. 2002;10(7):564-572. https://doi.org/10.1053/joca.2002.0814.
10. Holden PK, Liaw LH, Wong BJF. Human nasal cartilage ultrastructure: characteristics and comparison using scanning electron microscopy. *Laryngoscope*. 2008;118(7):1153-1156. https://doi.org/10.1097/MLG.0b013e31816ed5ad.
11. Sinclair S, Walsh WR. Characterization of costal cartilage allografts. *ANZ J Surg*. 2022;92(9):2274-2279. https://doi.org/10.1111/ans.17967.
12. Mansfield JC, Mandalia V, Toms A, Winlove CP, Brasselet S. Collagen reorganization in cartilage under strain probed by polarization sensitive second harmonic generation microscopy. *J R Soc Interface*. 2019;16(150):20180611. https://doi.org/10.1098/rsif.2018.0611.
13. Zhu W, Cao L, Song C, Pang Z, Jiang H, Guo C. Cell-derived decellularized extracellular matrix scaffolds for articular cartilage repair. *Int J Artif Organs*. 2021;44(4):269-281. https://doi.org/10.1177/0391398820953866.
14. Zevenbergen L, Gsell W, Cai L, et al. Cartilage-on-cartilage contact: effect of compressive loading on tissue deformations and structural integrity of bovine articular cartilage. *Osteoarthr Cartil*. 2018;26(12):1699-1709. https://doi.org/10.1016/j.joca.2018.08.009.
15. Huwe LW, Sullan GK, Hu JC, Athanasiou KA. Using costal chondrocytes to engineer articular cartilage with applications of passive axial compression and bioactive stimuli. *Tissue Eng Part A*. 2018;24(5–6):516-526. https://doi.org/10.1089/ten.tea.2017.0136.
16. Griffin MF, Premakumar Y, Seifalian AM, Szarko M, Butler PEM. Biomechanical characterisation of the human nasal cartilages; implications for tissue engineering. *J Mater Sci Mater Med*. 2016;27(1):11. https://doi.org/10.1007/s10856-015-5619-8.
17. Chen MH, Broom N. On the ultrastructure of softened cartilage: a possible model for structural transformation. *J Anat*. 1998;192(3):329-341. https://doi.org/10.1046/j.1469-7580.1998.19230329.x.
18. Hayes AJ, MacPherson S, Morrison H, Dowthwaite G, Archer CW. The development of articular cartilage: evidence for an appositional growth mechanism. *Anat Embryol (Berl)*. 2001;203(6):469-479. https://doi.org/10.1007/s004290100178.
19. Bos EJ, Pluemeekers M, Helder M, et al. Structural and mechanical comparison of human ear, alar, and septal cartilage. *Plast Reconstr Surg Glob Open*. 2018;6(1):e1610. https://doi.org/10.1097/GOX.0000000000001610.
20. Li Y, Chen X, Watkins B, et al. Nonlabeling and quantitative assessment of chondrocyte viability in articular cartilage with intrinsic nonlinear optical signatures. *Exp Biol Med*. 2020;245(4):348-359. https://doi.org/10.1177/1535370219896545.